

# Simulation of Damage Progression on Wind Turbine Blades Subject to Particle Erosion

Giovanni Fiore\* and Michael S. Selig†

*University of Illinois at Urbana-Champaign, Department of Aerospace Engineering, Urbana, IL 61801*

A time-marching code for predicting the evolving shape of wind turbine airfoils subject to erosion is discussed. The erosive damage to the blade surface was represented by sand grains colliding with the blade leading edge. The erosion rate was computed on the airfoil, and the damage depth was evaluated at each location. It was found that the locations of maximum erosion rate did not necessarily overlap with the locations of maximum eroded depth on the blade surface. In particular, the maximum damage depth was found very near the leading edge, and the results are in good agreement with photographic evidence. Three main phases were identified through the blade lifespan: an upper core breach, a lower core breach, and a leading edge core breach. A parametric study was performed in order to determine the most relevant drivers of the blade lifespan. In particular, the sand grain diameter was found to be the most significant driver, and the lifespan of the blade decreases parabolically as the grain diameter increases. Both the blade lift coefficient and the turbine hub height showed a direct relationship with blade lifespan. Large lift coefficients and large turbine hub heights are beneficial to increasing blade lifespan. It was also found that modern, large wind turbines are affected consistently less by sand erosion than small wind turbines. Such an effect is due to the increased influence of the blade flowfield toward a deviation of the incoming particles when large blade chord lengths are involved. Finally, a survey of various airfoil geometries allowed to identify the shape of the leading edge along with the airfoil aft camber as the primary drivers of blade section lifespan. The survey was performed by using the NREL S-airfoil family along with the tip-region airfoil DU 96-W-180. It was found that bulbous and round leading edges, coupled with moderately aft-cambered airfoils allowed for the longest blade lifespans, since they reduce the blade upper suction peak and offer steeper impact angles to the particles.

## Nomenclature

$A$	=	particle reference area
$AK$	=	particle nondimensional mass
$c$	=	airfoil chord length
$C_D$	=	particle drag coefficient
$C_l$	=	airfoil lift coefficient
$d$	=	particle diameter
$D$	=	particle drag force
$E$	=	erosion rate
$f$	=	sand grain shape factor
$h$	=	height
$h_0$	=	terrain roughness parameter
$H_V$	=	Vickers hardness
$K$	=	erosion rate constant
$m$	=	particle mass

---

\*Graduate Student (Ph.D.), Department of Aerospace Engineering, 104 S. Wright St., AIAA Student Member.

†Professor, Department of Aerospace Engineering, 104 S. Wright St., AIAA Associate Fellow.  
<http://m-selig.ae.illinois.edu/>

$M$	=	erodent mass flow rate
$n$	=	erosion rate velocity exponent
$N$	=	number of particle impacts per unit time
$r/R$	=	blade section radial location
$Re$	=	particle Reynolds number
$Re_\infty$	=	freestream Reynolds number
$s$	=	impact location relative to airfoil arc length
$t$	=	time
$t/c$	=	airfoil thickness-to-chord ratio
$U$	=	chordwise velocity component
$V$	=	chord-normal velocity component
$V_\infty$	=	freestream velocity
$V_r$	=	particle relative velocity
$V_{wind}$	=	wind velocity
$x$	=	particle $x$ -location
$y$	=	particle $y$ -location
$Z$	=	impedance
$\alpha$	=	angle of attack
$\alpha_r$	=	relative angle between the flowfield and particle velocity
$\beta$	=	impingement efficiency
$\delta$	=	damage depth
$\eta$	=	erosion efficiency parameter
$\lambda$	=	tip-speed ratio
$\theta$	=	impact angle
$\mu$	=	dynamic viscosity
$\rho$	=	density
$\tau$	=	nondimensional time
$\Omega$	=	wind turbine angular velocity
$\xi$	=	exponent of the wind power-law profile

#### *Acronyms*

COE	=	cost of energy
GAEP	=	gross annual energy production

#### *Subscripts and Superscripts*

0	=	initial state
$C$	=	coating
$hub$	=	turbine hub
$l$	=	lower side
$max$	=	maximum
$P$	=	particle
$r$	=	relative
$ref$	=	reference
$S$	=	sand
$u$	=	upper side
$V$	=	volumetric

## I. Introduction

Wind turbines used for electrical power generation are subject to fouling and damage by airborne particles typical of the environment where wind turbines operate. Throughout the 20-year lifespan of a wind turbine, particles such as rain, sand, hail, insects, and ice crystals are major contributors to a deterioration in turbine performance through local airfoil surface alterations.<sup>1-6</sup> Wind turbine blades accumulate dirt especially in the leading edge region. In addition,

temperature jumps and freeze-thaw cycles may cause smaller cracks in the coating to propagate, promoting coating removal and eventually delamination and corrosion damage due to exposure of the internal composite structure. The originally smooth surface of the blades may change considerably, and the increased roughness will cause a drop in gross annual energy production (GAEP) and an increase in cost of energy (COE).<sup>7-13</sup>

Modern trends in the wind turbine market have shown the benefits of offshore megawatt-scale turbine installations<sup>14,15</sup> in order to maximize GAEP while reducing COE. However, offshore locations are subject to more intense sand erosion than the majority of land installations.<sup>13,16,17</sup> Airborne sand particles collide with the blade and cause micro-cutting and plowing in the coating material<sup>18,19</sup> resulting in surface abrasion.<sup>20,21</sup> This type of damage is particularly prominent at the blade outboard sections where the local relative velocity is larger compared with inboard sections.<sup>16,22</sup>

The leading edge of a wind turbine blade is subject to slow shape modifications over time due to impacts with insects, hailstones, rain drops, and sand grains.<sup>22-26</sup> Within the damage scenario, however, the relevance of each type of particle is different. In fact, blade damage due to hailstones may be seen as a sporadic event in some locations around the world.<sup>16,27-29</sup> Similarly, insects are seldom capable of promoting actual blade damage, as opposed to just debris accretion.<sup>30,31</sup> The most consistent particles within the wind turbine erosion scenario are sand grains and rain drops. Of these two, sand grains represent the type of particle that is most subject to the aerodynamic influence of the blade due to their small weight.<sup>22,23</sup>

In aeronautics, a comparable problem to blade erosion over time is represented by wing icing.<sup>32</sup> In the icing problem, the characterization of the water content in the clouds and the relatively short time scale (order of minutes) allow for a computation of the ice accretion on a wing. Such simulation is then used to characterize the wing aerodynamic properties in icy conditions. However, the time scales involved with blade erosion may span anywhere from a few months to several years, depending on the weather conditions of a given wind farm and the air quality of such a location.<sup>33</sup> Moreover, as opposed to the icing problem, the air quality is not fully assessed at the wind turbine hub height, and the time scales involved are much longer. To this day, most sand sampling in the air is performed during specific sand storm events at a height near the ground,<sup>34-36</sup> or at cloud height by means of satellites.<sup>37</sup>

Monitoring the health of a blade surface is time consuming and detrimental toward both GAEP and COE.<sup>38,39</sup> Typically, the wind farm operator shuts down the turbine during pre-planned time slots while the maintenance operators photograph the blade surface from the ground by means of telephoto cameras. These photos are analyzed and a decision is made regarding blade repair, with additional costs associated with blade maintenance. From an aerodynamic standpoint, the location, depth, and roughness of the damaged areas drive the aerodynamic performance of the blade.<sup>40-42</sup> These motivations prove the importance of modeling and predicting the time-evolution of the blade section shape subject to particle damage.

This paper is divided into six Sections: the numerical method used is explained in Section II, the wind turbine operating conditions are introduced in Section III, the simulation setup is introduced in Section IV, the parametric studies and results are discussed in Section V, and conclusions are presented in Section VI.

## II. Methodology and Theoretical Development

### A. Particle Equations of Motion

In order to predict the erosive effect of sand grains onto the blade surface, a Lagrangian formulation code was developed in-house and named BugFoil.<sup>22,23</sup> BugFoil integrates a pre-existing particle trajectory code<sup>43</sup> and a customized version of XFOIL.<sup>44</sup> The local flowfield velocity components are obtained by querying the built-in potential flow routine of XFOIL from which the particle trajectory and impact location on the airfoil are computed.

In steady flight, the forces acting on the particle are perfectly balanced and perturbations to such forces are assumed to be additive to the steady-state forces. For these reasons the equations of motion may be expressed by neglecting the steady-state forces and may be written as functions of increments only.<sup>45</sup> In the current study, both raindrops and hailstones were treated as aerodynamic bodies whose only associated force is the aerodynamic drag  $D$ .

By applying Newton's second law along the particle trajectory in both chordwise  $x$  and chord-normal  $y$  directions,

the following equations are obtained<sup>18,22,32,46,47</sup>

$$m_P \frac{d^2 x_P}{dt^2} = \Sigma F_x \quad (1)$$

$$m_P \frac{d^2 y_P}{dt^2} = \Sigma F_y \quad (2)$$

By projecting the drag of the particle  $D$  in both chordwise  $x$  and chord-normal  $y$  directions using the relative angle between particle and flowfield velocity  $\alpha_r$ , the equations may be rewritten as

$$m_P \frac{d^2 x_P}{dt^2} = \Delta D \cos \alpha_r \quad (3)$$

$$m_P \frac{d^2 y_P}{dt^2} = \Delta D \sin \alpha_r \quad (4)$$

Given the particle velocity components  $U_P$  and  $V_P$  and given the velocity flowfield components  $U$  and  $V$  at a certain point along the trajectory, the particle slip velocity  $V_s$  can be expressed as

$$V_s = \sqrt{(U - U_P)^2 + (V - V_P)^2} \quad (5)$$

while the trigonometric functions in Eqs. 3 and 4 may assume the form

$$\cos \alpha_r = \frac{U - U_P}{V_s} = \frac{V_{rx}}{V_s} \quad (6)$$

$$\sin \alpha_r = \frac{V - V_P}{V_s} = \frac{V_{ry}}{V_s} \quad (7)$$

By expressing the particle aerodynamic drag  $D$  as a function of dynamic pressure and by substituting for the trigonometric functions, the Eqs. 3 and 4 may be rewritten as

$$m_P \frac{d^2 x_P}{dt^2} = \frac{1}{2} \rho V_s^2 A_P C_D \frac{V_{rx}}{V_s} \quad (8)$$

$$m_P \frac{d^2 y_P}{dt^2} = \frac{1}{2} \rho V_s^2 A_P C_D \frac{V_{ry}}{V_s} \quad (9)$$

To scale this problem in a non-dimensional fashion, non-dimensional time, space, and mass parameters can be introduced here

$$\tau = \frac{t U}{c} \quad (10)$$

$$\bar{x}_P = \frac{x_P}{c} \quad (11)$$

$$\bar{y}_P = \frac{y_P}{c} \quad (12)$$

$$AK = \frac{2 m_P}{\rho A_P c} \quad (13)$$

Nondimensionalization of Eqs. 8 and 9 by a reference velocity  $U$  yield

$$\frac{d^2 \bar{x}_P}{d\tau^2} = \frac{1}{AK} \bar{V}_r C_D \bar{V}_{rx} \quad (14)$$

$$\frac{d^2 \bar{y}_P}{d\tau^2} = \frac{1}{AK} \bar{V}_r C_D \bar{V}_{ry} \quad (15)$$

which together represent a set of second-order, nonlinear differential equations. Once the particle drag coefficient is evaluated, the trajectory can be computed by numerically solving both  $x$  and  $y$  equations.

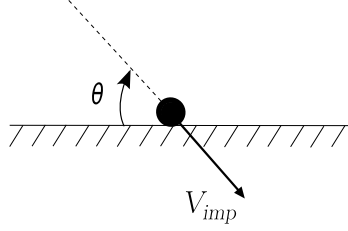


Figure 1. Impact velocity  $V_{imp}$  and impact angle  $\theta$  with respect to blade surface.

## B. Aerodynamics of the Sand Grain

Airborne sand particles are mainly represented by silica-based grains. To incorporate shape irregularities typical of sand grains, the aerodynamic drag is modeled by means of a shape factor  $f$  defined as<sup>48</sup>

$$f = \frac{a}{A_S} \quad (16)$$

where  $a$  is the surface area of a sphere with the same volume of the sand grain, and  $A_S$  is the actual surface of the sand grain. Note that for perfectly spherical particles the shape factor is equal to unity. The drag coefficient for a sand grain is written in the form given by<sup>48</sup>

$$C_D = \frac{24}{Re_r} \left( 1 + b_1 Re_r^{b_2} \right) + \frac{b_3}{1 + \frac{b_4}{Re_r}} \quad (17)$$

where the  $b_i$  coefficients are functions of  $f$ , and  $Re_r$  is the relative Reynolds number defined as

$$Re_r = \frac{\rho d_S |U_S - U|}{\mu} \quad (18)$$

The aerodynamic drag force can be expressed as<sup>17,47</sup>

$$D = \frac{18 \mu C_D Re_r}{\rho_S d_S^2} \quad (19)$$

In the current study, the sand grain lift coefficient is assumed to be negligible.

## C. Sand Erosion

Sand erosion has been investigated for a variety of air-breathing engines in aerospace applications.<sup>21,47,49,50</sup> Sand grain velocities in those applications are in the same range of the wind turbine erosion scenario. Typically, erosion is responsible for an increase in blade surface roughness and a decrease in structural stiffness. The parameter erosion rate  $E$ , defined as the removed mass of the target material divided by the mass of the impacting particle, is a function of the particle impact velocity  $V_{imp}$  and angle at impact  $\theta$  (as defined in Fig. 1), and it is measured in the practical units of (g/g).<sup>19</sup> The impact velocity is related to  $E$  through a power-law; whereas, the correlation with impact angle strongly depends on the eroded material properties. Erosion is characterized by two contributions, a plastic and a brittle erosion mode,<sup>18,19</sup> depending on the value of  $\theta$  at which  $E$  is maximum. Most current materials used for wind blade coating are polyurethane derivatives<sup>38</sup> and show a primarily plastic erosion behavior with maximum erosion rate at  $\theta = 30$  deg.<sup>51</sup> A common way to model the erosion rate for plastic materials is given by the equation<sup>20,50,52–54</sup>

$$E = K V_{imp}^n \quad (20)$$

where  $K$  and  $n$  are constants of the eroded material. The correlation between  $E$  and  $\theta$  is implicit in the parameters  $K$  and  $n$  that are fitted at various impact angles and impact velocities.

Unfortunately, there is a lack of experimental data on polyurethane erosion at various impact velocities.<sup>55</sup> At present, most of the erosion experimental research is aimed at characterizing polyethylene-based coatings, which have

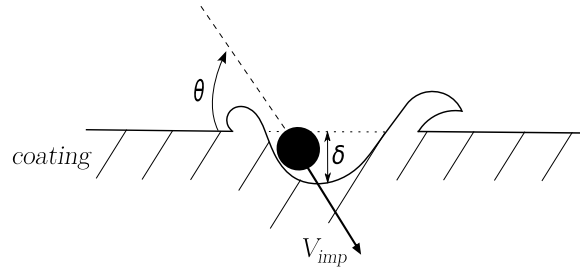


**Figure 2.** Volume loss and volume displacement of a plastic material due to impact with sand grains ( $\delta$  – damage depth).

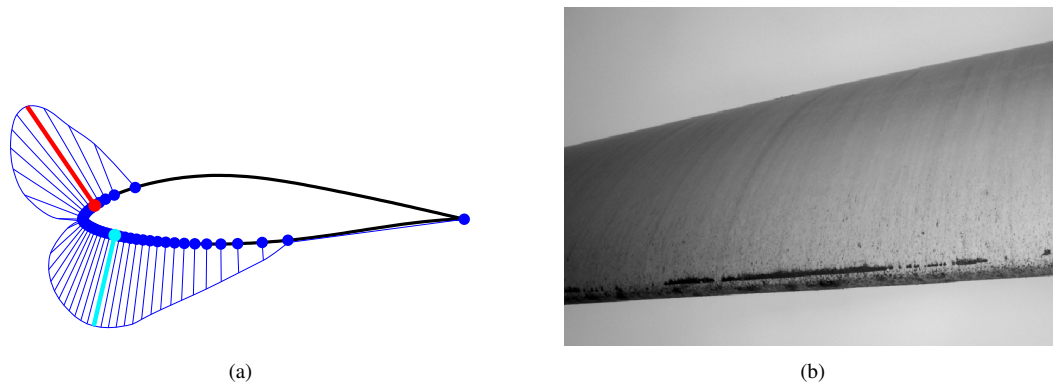


**Figure 3.** Computed erosion rate versus real-life sand damage: (a) the curves of erosion rate on a DU 96-W-180 airfoil,  $\alpha = 6.0$  deg. Red segment: upper maximum erosion rate; cyan segment: lower maximum erosion rate; blue circles: particle impingement points; and (b) a real-life blade showing the signature of sand grain erosion, the black areas represent the maximum eroded depth.

a similar erosion behavior compared with polyurethane.<sup>51</sup> For these reasons, the simulations were performed by using linear-fitted erosion constants for ultrahigh molecular weight polyethylene (UHMWPE),<sup>22</sup> so UHMWPE was used because it has the best performance of the polyethylene-based coatings.<sup>52</sup>

Each simulation is performed by placing a vertical array of sand particles five chord lengths upstream of the airfoil. Once the simulation is initiated, the trajectory of the particles is evaluated and impingement is estimated. Given the angle and velocity at impact,  $E$  takes different values in the region around the leading edge, with a minimum associated with near-normal impact. The erosion rate  $E$  curves due to sand on a DU 96-W-180 airfoil ( $\alpha = 6.0$  deg) are shown in Fig. 3(a).<sup>22</sup> The peaks of  $E$  are located downstream of the LE on both upper and lower surfaces and their location depends on the blade angle of attack, particle size, and inflow velocity.<sup>41</sup>

#### D. Damage Depth

Blade coating materials show a typical plastic behavior that is of fundamental importance when considering the damage promoted by sand grains onto the blade surface. Experiments have shown that such materials are not only subject to volume loss, but also to volume displacement when subject to erosive particles, as shown in Fig. 2.<sup>56</sup> In other words, even though a plastic material may look eroded after an erosion test due to volume loss, the weight of such sample would not be accordingly reduced due to a volume displacement. This effect implies that the shape of the erosion rate curve may substantially differ from the curve of the erosion depth on a given blade section. By inspecting Fig. 3 it is evident that the locations of maximum  $E$  [Fig. 3(a)] appear significantly more downstream than the locations of maximum erosive depth [Fig. 3(b)]. Thus, it is of paramount importance to predict the locations of maximum surface displacement and relate them to the curves of the erosion rate  $E$ .

In the current study, the approach investigated by Patnaik et al. is implemented in order to predict the damage depth  $\delta$  on the blade surface due to sand particles.<sup>56</sup> To take into account the volume of removed material as opposed

to the volume of displaced material, the erosion efficiency parameter  $\eta$  is introduced as

$$\eta = \frac{2 E H_V}{\rho_S V_{imp}^2 \sin^2 \theta} \quad (21)$$

where  $H_V$  is the Vickers hardness of the target material,  $\rho_S$  is the erodent density (sand),  $\theta$  is the particle impact angle, and  $V_{imp}$  is the particle velocity at impact (see Fig. 2). When  $\eta = 1$  there exists a direct relationship between removed volume and displaced volume. At that point all the displaced volume is also removed. For values of  $\eta$  smaller than one, the material is subject to volume displacement and not all the material is being removed from the surface.

Given the impact of a particle onto a plastic surface, the volumetric loss of material can be expressed as

$$E_V = \frac{\pi}{2} d_S \delta^2 N \eta \quad (22)$$

where  $d_S$  is the sand grain diameter,  $\delta$  is the damage depth due to a single particle, and  $N$  is the number of particle impacts per unit time. The term  $N$  can be derived from the erodent mass flow rate  $M$ , by

$$N = \frac{M}{\frac{\pi d_S^3}{6} \rho_S} \quad (23)$$

and by noting that the volumetric loss  $E_V$  of the coating (C) can be expressed by

$$E_V = \frac{M E}{\rho_C} \quad (24)$$

Equation 22 can be used to derive the damage depth  $\delta$  (shown in Fig. 2) as

$$\delta = \sqrt{\frac{2 E_V}{\pi d_S N \eta}} = \sqrt{\frac{2 \frac{M E}{\rho_C}}{\pi d_S \frac{M}{\frac{\pi d_S^3}{6} \rho_S} \eta}} = d_S \sqrt{\frac{1}{3} \frac{\rho_S}{\rho_C} \frac{E}{\eta}} \quad (25)$$

Once the erosion rate  $E$  is computed, the damage depth  $\delta$  due to a single particle onto the surface can be computed by knowing the coating and sand density ( $\rho_C$  and  $\rho_S$ , respectively), the particle diameter  $d_S$ , and the erosion efficiency  $\eta$ . In this context, evaluating  $\delta$  can be regarded as computing the surface displacement resulting from mass and volume removal.

### III. Wind Turbine Operating Conditions

The characteristics of the air surrounding a wind turbine play a crucial role in the shape modifications of the blade over time. In previous studies, it was observed that the sand grain size drives the morphology of the erosion rate curves on an airfoil.<sup>22,41</sup> In particular, large particles are responsible for high peaks, and large impact envelopes of  $E$  over the airfoil, as opposed to lightweight particles that promote small peaks and small impact envelopes of  $E$ . Therefore, an estimate of the sand grain diameter at the blade height needs to be made for accurate predictions of airfoil shape modifications over time.

#### A. Sand Characteristics

Sand grains are subject to natural aeolian transportation due to winds blowing over the majority of the surface of the earth. However small, sand grains are characterized by inertia, so the capability of the wind to transport such particles to a given height is related to the particle mass. Therefore, large and heavy particles are observed in the proximity of the ground; whereas, small and lightweight particles can be carried at much higher altitudes and for longer distances.<sup>34–36</sup> In particular, it was observed that a logarithmic relationship exists between the sand grain diameter and transport

height. Li et al. provide an expression for the sand grain diameter  $d_S$  at a given height  $h$  by means of a reference sand grain diameter  $d_{S,0}$  at sea level,<sup>35</sup> hence

$$d_S = d_{S,0} h^{-0.155} \quad (26)$$

Thus, for any given blade height across its revolving motion, the sand grain diameter can be computed.

The variation in particle size experienced by a given blade section across the entire revolution is a function of the rotor diameter and hub height. Pitch regulated wind turbines with high power ratings will experience a larger variation in particle diameter from the blade lowest height to the highest, as compared with small, stall regulated wind turbines. This consideration is especially true for very large, offshore wind turbines, associated with higher power ratings and large rotor diameters.<sup>13,15,25</sup>

Given a blade rotating about the hub, placed at a height  $h_{hub}$  off the ground, the height of a given spanwise location is given by

$$h = h_{hub} + r \sin\left(\frac{2\pi}{60} \Omega t\right) \quad (27)$$

where  $r$  is the blade span location, and  $\Omega$  is the turbine rotational speed in rpm. Once  $h$  is fixed, the particle diameter at that height is computed by using Eq. 26.

## B. Wind Characteristics

The erosion rate  $E$  due to sand particles impacting on a plastic material surface is approximately related to the third power of the particle impact velocity  $V_{imp}$ .<sup>22,41</sup> Hence, variations in wind speed  $V_{wind}$  may contribute significantly to the erosive damage on the blade surface. It is a well known fact that the wind blowing across the surface of the earth can be approximated with a parabolic profile.<sup>57</sup> Moreover, the curvature of such profile is related to the type of terrain, and it is typically more pronounced for urban environment. In contrast, more uniform wind profiles are observed for flat, countryside areas, and for offshore environments.

In order to compute the intensity of the wind at a given height  $h$ , the approach used in the current study is taken from Spera et al.<sup>57</sup> The wind profile is defined through a power law, viz

$$V_{wind} = V_{wind,ref} \left(\frac{h}{h_{ref}}\right)^\xi \quad (28)$$

where  $V_{wind,ref}$  is the reference wind speed at the reference height  $h_{ref}$  (typically equal to 10 m). The exponent  $\xi$  is expressed through

$$\xi = \xi_0 [1 - 0.55 \log(V_{wind,ref})] \quad (29)$$

where  $\xi_0$  is written as

$$\xi = \left(\frac{h_0}{10}\right)^{0.2} \quad (30)$$

and  $h_0$  is a parameter related to the terrain roughness. Typical values of  $h_0$  span from the flat countryside where  $h_0 = 0.002 - 0.3$ , to urban and city environments where  $h_0 = 0.4 - 3.0$ .<sup>57</sup> For the current simulations, a flat terrain was assumed, taking  $h_0 = 0.002$  typical of flat terrains. Similar to the sand grain diameter, once the blade height  $h$  is fixed, the wind speed  $V_{wind}$  is also fixed by using Eq. 28.

## IV. Simulation Setup

The time marching code is run by simulating subsequent erosive events. Each event is intended as a frozen-condition simulation, in which the blade height  $h$  is computed at a prescribed instant (see Eq. 27), thus the particle diameter  $d_S$ , and wind speed  $V_{wind}$  are determined by using Eqs. 26 and 28, respectively. In this context, the simulations are based on pseudo time and representative of instances of erosion each damaging and removing material from the blade surface. Such an approach can be regarded as quasi-steady, in which the time scale of the erosive event is much shorter

than the time scale associated with the blade motion.

Given the mathematical method discussed in Sec. III A, the challenge is now on setting up a realistic scenario for predicting the airfoil shape after a given amount of time. However, the uncertainty that currently exists in characterizing the quantity of atmospheric particles for a given geographic location makes it difficult to predict a unique airfoil shape subject to particle erosion.

Since the erosion depth  $\delta$  is directly related to the particle diameter  $d_S$  (see Eq. 25), the final shape of a wind turbine blade section depends on the history of the erosive events throughout its lifespan. For such a reason, the three blades of a given turbine will experience different erosion histories due to the impact of sand particles at different blade heights. This consideration is reflected into different geometries of the eroded leading edges within the same wind turbine, operating in the same geographic location. Because the history of erosive events dictates the final airfoil shape, and because no existing data can be used to model the amount of sand of a given location, the erosive history of the blade is arbitrarily assigned.

To ensure repeatability of the results, the chosen approach is through a wind turbine clock-function. The possible blade positions are obtained by discretizing the circular angle into several angular slices 17 degrees wide. The blade can only occupy a position dictated by the slices and by doing so it will occupy a uniform variety of positions as the number of revolutions increases, as shown in Fig. 4. Once the clock-function assigns the blade angular slice, the algorithm evaluates the height off the ground  $h$ , the windspeed  $V_{wind}$ , the particle diameter  $d_S$ , and the nondimensional particle mass parameter  $AK$ . At that point the computation of the erosion depth  $\delta$  is initiated.

The uneroded blade section is modeled by a coating surface shaped as an airfoil, under which the core material exists, as shown in Fig. 5. A 1 mm UHMWPE coating is chosen for the present simulations, since typical coating thicknesses are in the range of  $\approx 0.5$ – $1.5$  mm. Throughout the current, work the initial uneroded conditions will be called Phase 0.

The high-level flowchart of the code is as follows:

1. The blade section geometry is fed into XFOIL as a typical geometry text file, and the inviscid flowfield is computed at a given angle of attack  $\alpha$ .
2. BugFoil is used to compute the trajectory of the sand grains over the airfoil, and the erosion rate  $E$  is computed at the locations of particle impact.
3. The local erosion depth  $\delta$  is computed by using  $E$  at that impact location (see Eq. 25).
4.  $\delta$  is interpolated onto the geometry nodes, and the airfoil geometry is updated (eroded).
5. Updated geometry is saved into a separate time-stamped geometry file.
6. The code goes back to step 1 until the stop criteria is matched.

After a certain number of erosive events (pseudo elapsed time), when no coating is present at a given node of the geometry, the code uses red markers on the geometry output on screen, as shown in Fig. 6. Since such event is significant to predict the blade lifespan, the event of no coating on a given node will be regarded as core breach.

It should be noted that each erosive event is responsible for a surface displacement  $\delta$  on the order of micrometers. Such a consideration is important when estimating the computational time to simulate the core breach on a blade section geometry.

## A. Erosion Phases

Multiple simulations were performed by varying airfoil geometry, coating thickness, angle of attack and particle size. For every case, a consistent erosive pattern was found and four relevant phases were isolated, as shown in Fig. 7. They can be summarized as:

1. Phase 1 – upper core breach: the first instance of coating removal appears on the upper side of the leading edge [Fig. 7(a)]. This is because the high velocity of the flowfield on the upper side of the leading edge promotes higher erosion rates when compared with the lower side
2. Phase 2 – lower core breach: the first instance of coating removal appears also on the lower side of the leading edge [Fig. 7(b)]. Also, a narrow residual coating is present at the forwardmost point of the leading edge, while erosion progressed into the core on the upper side

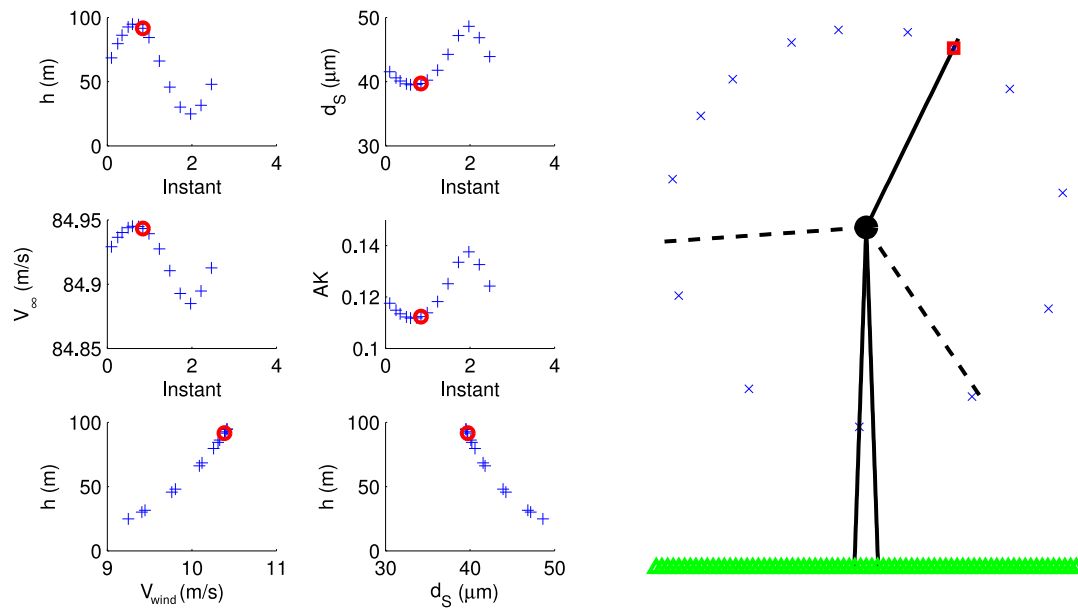


Figure 4. The wind turbine clock-function during a time-stepping simulation. In red the conditions being simulated at that instance, in blue the conditions simulated in previous instances.

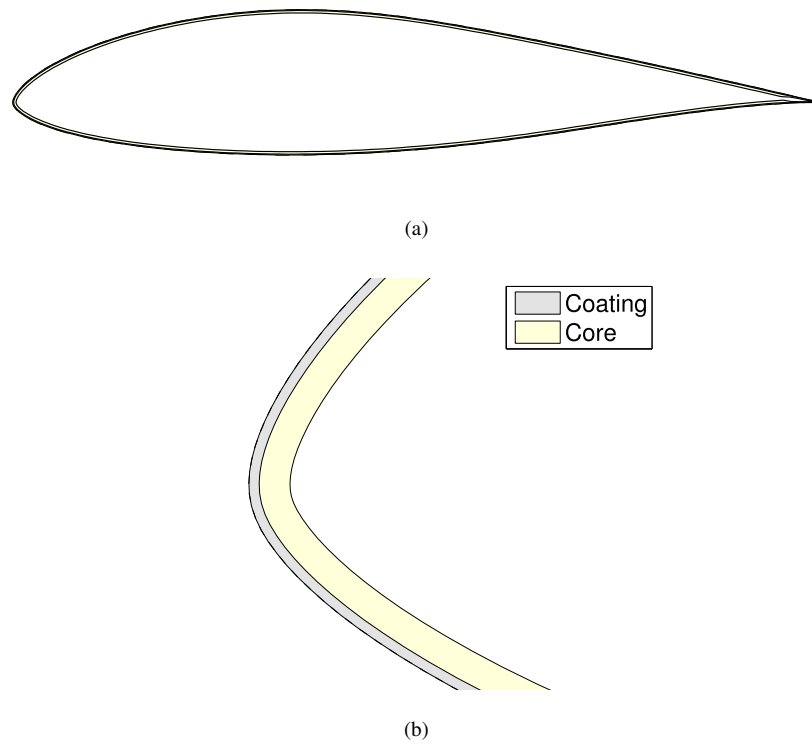


Figure 5. Layout of a new, uneroded airfoil (Phase 0): (a) overview, and (b) zoom-in.

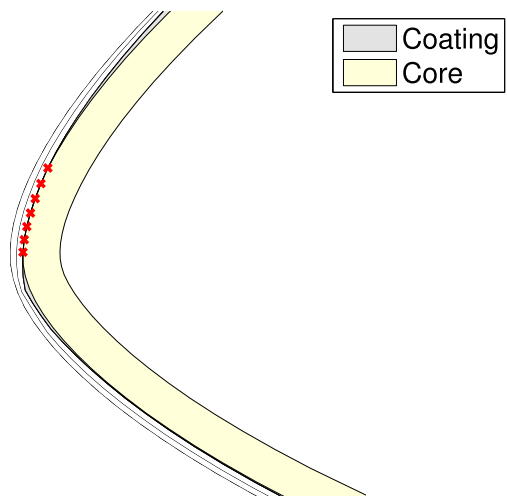


Figure 6. Core breach is shown by red markers during the time marching simulations; note that the surface displacement for each erosive event has been intentionally augmented for displaying purposes.

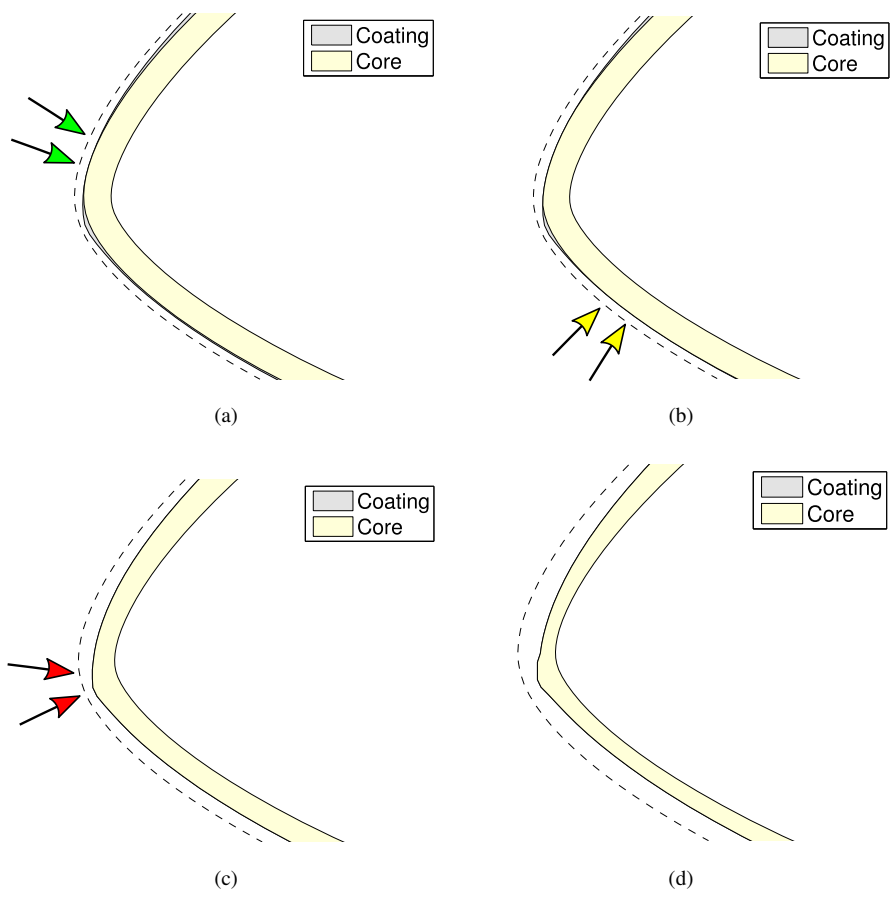


Figure 7. Erosive phases: (a) Phase 1 – upper core breach, (b) Phase 2 – lower core breach, (c) Phase 3 – leading edge core breach, and (d) Phase 4 – advanced erosion.



(a)



(b)



(c)



(d)

**Figure 8. Photographic evidence of the erosive phases: (a) Phase 1 – upper core breach (Ref. 58), (b) Phase 2 – lower core breach (Ref. 59), (c) Phase 3 – leading edge core breach (Ref. 60), and (d) Phase 4 – advanced erosion (note the small bump in the leading edge) (Ref. 61).**

3. Phase 3 – leading edge core breach: the residual coating is removed and the leading edge is now left uncoated [Fig. 7(c)]. The erosion has progressed onto the upper and lower side of the airfoil
4. Phase 4 – advanced erosion: the sand erosion progresses onto the core along the entire leading edge [Fig. 7(d)], and a small bump in the core material appears where the aerodynamic stagnation point is.

The erosion phases are color coded throughout this paper based on their severity. In particular, green is assigned to Phase 1, yellow to Phase 2, and red to Phase 3. Moreover, in figures to be presented later, the upper core breach is associated with a top-up triangle marker, the lower core breach is associated with a top-down triangle marker, and the leading edge core breach is associated with a square marker.

Due to the novelty of the present analysis, a validation of results would require knowing the history of erosive events for a given wind turbine blade. In particular, the diameter of the particles, the shape of the airfoil, and the depth of damage would have to be recorded at fixed periods and monitored over a time interval in the range of several years. For such reasons, a qualitative comparison with photographic evidence is performed, as shown in Fig. 8. The similarity with the simulations is striking (shown in Fig. 7), and for the first time in this field a time collocation of the erosive phases of a wind turbine blade is performed.

At present, the research by Corsini et al.<sup>62</sup> represents the only document found in the literature that describes a similar erosive pattern for airfoils. In their work, the fan of an actual turbomachinery was investigated to characterize blade erosion due to quartz particles. It was noticed that minimum erosion existed at the forwardmost point of the leading edge, and two main regions of removed material were found on the upper and lower sides of the airfoil just downstream of the leading edge. Such information represents a qualitative agreement with the results found in the current work.

## V. Parametric Studies – Results and Discussion

The time-stepping simulation tool allows for a great variety of novel studies to be performed. In general, it would be particularly interesting to characterize the blade section based on a time scale, as a sequence of erosive phases. Hence, in this Section the term lifetime will be regarded as the number of erosive events before reaching a particular erosive phase. However, in order to isolate the effects of a single parameter on the lifetime of a blade section, only one input at a time will be changed, similar to the approach used in previous studies.<sup>41</sup>

Since each parametric study will be compared to the baseline case, a clever way to highlight differences in lifetime is by selecting a small sand grain diameter as the baseline, thus  $d_{s,0} = 80 \mu\text{m}$ . In fact, by inspecting Eq. 25, it can be noticed that the particle diameter drives directly the surface displacement  $\delta$ . Hence, by simulating the erosion due to small particles, the number of erosive events to achieve a particular phase is more finely resolved when compared with larger particles.

The computational time of the time-stepping simulations varies from case to case. Depending on the blade conditions, airfoil geometry, and particle size, the number of erosive events may substantially vary, in order to reach the same erosive phase. The computations were performed on a desktop PC and required an average of 1 hr of CPU to simulate erosion to Phase 3, and at that point the simulation is stopped.

Throughout the current Section, the presented charts show the blade section lifetime versus the specific parameter that is being varied. Because Phase 1 through Phase 3 can be thought as distinctive phases of the erosive process of the blade, they will be distinctively marked with the color/marker code explained in the previous Section. The parametric studies that follow compare the lifetime of blade sections located at  $r/R = 0.95$  for several different conditions (variable  $C_l$ ,  $d_s$ ,  $h_{hub}$ , turbine rated power, and airfoil geometry) and mounted on the HAWT baseline configuration (1.5 MW,  $\lambda = 8.7$ ,  $R = 37$  m,  $h_{hub} = 60$  m,  $V_{wind} = 10$  m/s,  $c = 1$  m, 1 mm thick UHMWPE coating, unless otherwise stated).

### A. Effect of $C_l$ on Blade Lifetime

Depending on the wind intensity and the blade pitch, the aerodynamic angle of attack of the blade may vary substantially, and thus so too the blade section lift coefficient  $C_l$ .<sup>63</sup> Typically, high-wind days are associated with high angles of attack; whereas, low-wind days show low angles of attack. Pitch regulated HAWTs account for such variations by adjusting the blade pitch to operate at the design  $C_l$ . However, wind gusts during sand storms may be abrupt, and the pitch mechanism may fail to promptly adjust the blade angle of attack. In other words, the blade may operate at high  $C_l$  values that typically fall out of the design range.

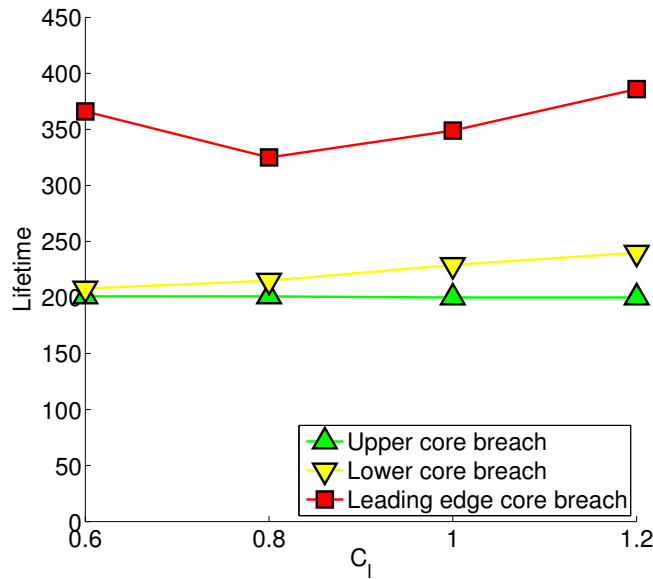


**Figure 9. Blade section lifetime versus lift coefficient**

From an aerodynamic standpoint,  $C_l$  drives the distribution of pressures over an airfoil. Since the aerodynamic angle of attack drives the intensity of the suction peak on the blade upper surface and the size of the the high-pressure region on the blade lower surface, it is relevant to investigate the effect of  $C_l$  with respect to blade lifetime. In particular, a DU 96-W-180 airfoil is tested for a range of  $C_l = 0.6 - 1.2$ .

Figure 9 shows the lifetime of the airfoil for variable  $C_l$ . In the current paper, lifetime is intended as the number of erosive events to reach a particular erosive Phase. It can be seen that the lifetime before the upper core breach does not display a strong dependence on  $C_l$ ; whereas, the lifetime before the lower core breach is more influenced. The increased high pressure area at high  $C_l$  allows the particle to slow down more and impact at a steeper angle on the airfoil lower side, hence increasing the number of erosive events it takes to reach Phase 2. A similar reason lies behind the increase in lifetime before the leading edge core breach (Phase 3) at high values of  $C_l$ . At  $C_l = 0.6$  a high lifetime before Phase 3 is observed, and it is due to the quasi-perpendicular impact of the particles with the leading edge, thus reducing the surface displacement  $\delta$  for each particle impact.

The current parametric study shows that it may be beneficial towards blade lifetime to operate at high  $C_l$ , and hence high angles of attack. In particular, Phase 3 shows the most benefits when  $C_l$  is increased. However, it should be noted that operating a blade at high  $C_l$  values is not necessarily beneficial toward  $C_l/C_d$ , and a trade off should be performed. Moreover, a high  $C_l$  is associated with a high  $\alpha$ , thus potentially exposing the blade lower side to the erosion of heavy particles, such as hailstones and raindrops, as previously investigated in Ref. 41.

## B. Effect of Particle Size on Blade Lifetime

In a previous study, it was noticed that the particle mass substantially drives the erosion rate  $E$  observed on an airfoil.<sup>41</sup> Depending on the geographic location of the wind turbine, the size of the sand grains may vary considerably. Severe sand storms may also transport significantly larger particles than usually observed at a given location.<sup>36,37</sup> Currently, no readily available scientific data exists to assess the sand grain diameter at the wind turbine operating height, as explained in the introduction of the current Section. However, the research on helicopter engine erosion reported  $200 \mu\text{m}$  as a typical sand grain diameter in ground proximity for desertic regions.<sup>47</sup> On the other hand, diameters of approximately  $5 \mu\text{m}$  were recorded by means of satellites in the hovering clouds above the desertic regions of China.<sup>34</sup> Because of such uncertainty, a parametric study based on sand grain diameter is here performed, where  $d_{s,0} = 80 - 640 \mu\text{m}$ .

Figure 10 shows the lifetime of a blade section located at  $r/R = 0.95$ , characterized by a DU 96-W-180 airfoil, and operating at  $C_l = 1.0$  for variable  $d_{s,0}$ . The lifetime before the upper, lower and leading edge core breach decreases

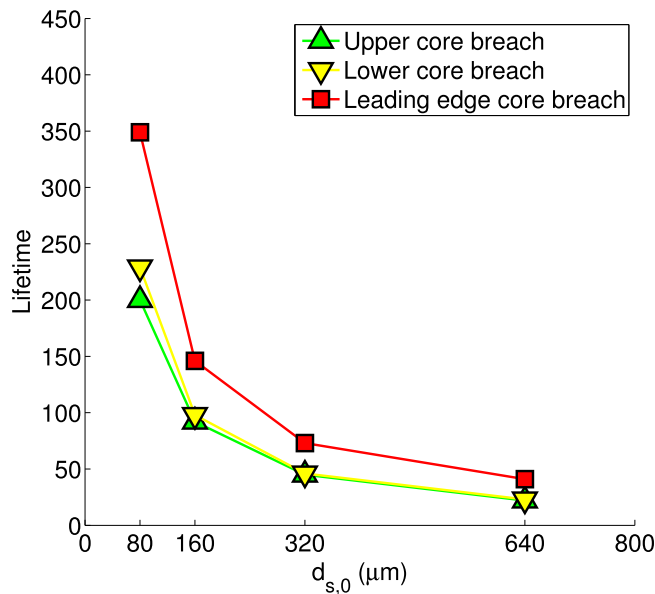


**Figure 10. Blade section lifetime versus sand grain diameter**

parabolically with increasing particle diameter. It is worth noticing that a somewhat consistent ratio between the lifetime phases exists regardless of the particle diameter. On the other hand, it should be also noted that the lifetime before the upper and lower core breach become similar as the particle increases in diameter. This effect is due to the increased inertia of the sand grain which will be progressively less affected by the aerodynamic flowfield around the blade, regardless of the impact on the upper or lower side of the airfoil.

In the present Section, the sand grain diameter appears to be one of the most relevant drivers with respect to blade section lifetime. Given two wind turbines manufactured by the same company, the lifetime observed at two different locations around the world may vary dramatically due to differences in sand grain diameter. The current uncertainties with respect to airborne particle characterization at the wind turbine hub height should be addressed to properly predict the lifetime of wind turbine blades. Such a conclusion calls for detailed investigations of the operating environment at wind farm sites.

### C. Effect of Hub Height on Blade Lifetime

Within the atmosphere of the earth, large sand particles are observed close to the ground and progressively smaller particles are observed as the height increases, as explained in Sec. III A. Such a characteristic of the atmosphere needs to be interfaced with the wind turbine operating height. Different manufacturers use different tower heights for very similar rated powers, based on the materials used, and their technical know-how. Moreover, the blade clearance is often regulated by country-specific laws to ensure safety. It is therefore relevant to investigate the role of the turbine hub height with respect to blade section lifetime. In the current parametric study only the turbine hub height is varied, and the turbine rated power, rotor diameter, tip-speed ratio, and chord length are held constant, as shown in Fig. 11(a).

Starting from the reference hub height (60 m), the investigated range of turbine hub height is  $h_{hub} = 50 \text{ m} - 80 \text{ m}$ , and the blade section considered is again characterized by the DU 96-W-180 airfoil, operating at  $C_l = 1.0$  and located at  $r/R = 0.95$ . In Fig. 11(b) it is shown the lifetime of the blade section with respect to  $h_{hub}$ . A direct correlation with  $h_{hub}$  is observed, and high elevations are beneficial with respect to blade lifetime. It has to be considered that such a benefit results from a smaller average sand grain diameter encountered at high elevations, despite the stronger wind intensity, as explained in Sec. III B. Finally, consistent benefits towards an increase in lifespan are observed for each erosive phase. It can be concluded that an increase in the tower height is beneficial with respect to blade lifespan and it could be readily used as a design factor for modifying existing turbine specifications.

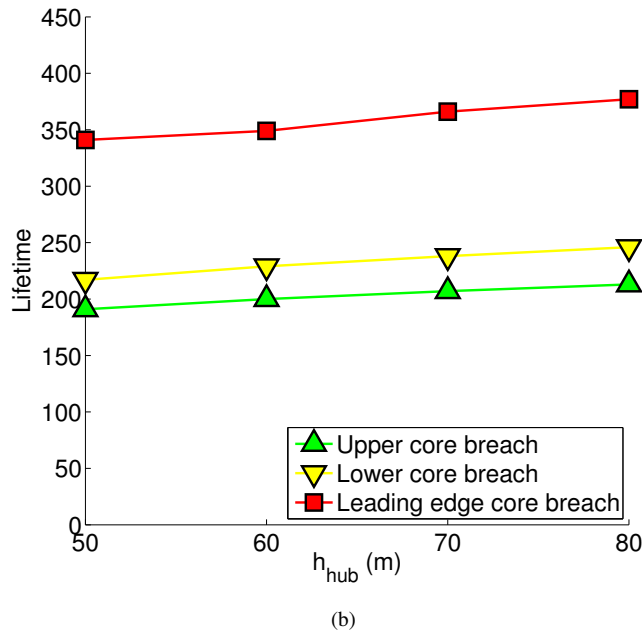
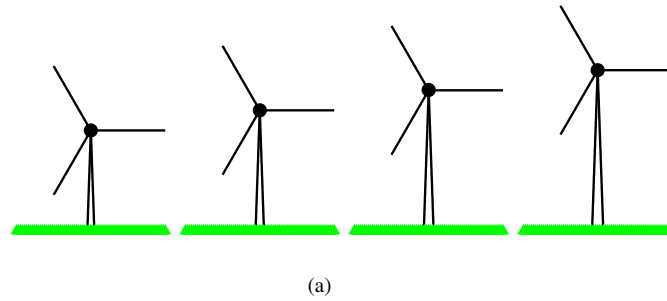


Figure 11. Hub height parametric study: (a) investigated turbine hub heights, from left to right  $h_{hub} = 50, 60, 70,$  and  $80$  m, and (b) blade section lifetime versus turbine hub height.

#### D. Effect of Wind Turbine Size on Blade Lifetime

The modern trends in the wind turbine commercial market see increasingly higher rated powers along with larger rotor diameters. In particular, typical rated powers of the mid-80's were in the range of 0.2 – 0.6 MW; whereas, modern wind turbines are capable of 2 – 3 MW of rated power.<sup>24,64,65</sup> New wind turbines are larger in every sense than older-generation wind turbines: larger rotor diameters, larger hub heights, and larger chord lengths. However, the tip-speed ratio is held constant through the scaling in order for the blade section to operate at a specific range of Reynolds numbers.

In the current Section, the lifetime of four wind turbines is compared. Starting from the baseline configuration of 1.5 MW,  $\lambda = 8.7$  HAWT, a geometric scaling has been performed to obtain the hub height, rotor diameter, and blade chord length for the other turbines. As a reference, the geometric specifications of two Siemens wind turbines are also used in the present study.<sup>65</sup> Since the turbine tip-speed ratio is held constant, the turbine angular velocity  $\Omega$  can be readily computed. It should be noted that the coating thickness is not geometrically scaled but it is held constant since it is believed that the coating procedure is not affected by the overall blade size. In other words, the industrial process of blade coating may not be a scalable factor. Thus, all simulations are performed with a 1 mm UHMWPE coating applied onto the blade surface, described by a DU 96-W-180 airfoil, operating at  $C_l = 1.0$ , and located at  $r/R = 0.95$ . The characteristics of each turbine are reported in Table 1.

Figure 12(a) shows the dimensions of the wind turbines relative to each other. The lifetime of the blades subject to

**Table 1. Specifications of the Wind Turbines for the Wind Turbine Size Parametric Study**

Rated Power (MW)	$h_{hub}$ (m)	$V_{wind}$ (m/s)	$R$ (m)	$\Omega$ (rpm)	$c @ (r/R)_{0.95}$ (m)
0.5	30	9.4	20	43.6	0.53
1.5	60	10.0	37	23.0	1.00
3.6	88	10.3	58	14.8	1.55
6.0	116	10.6	77	11.4	2.03

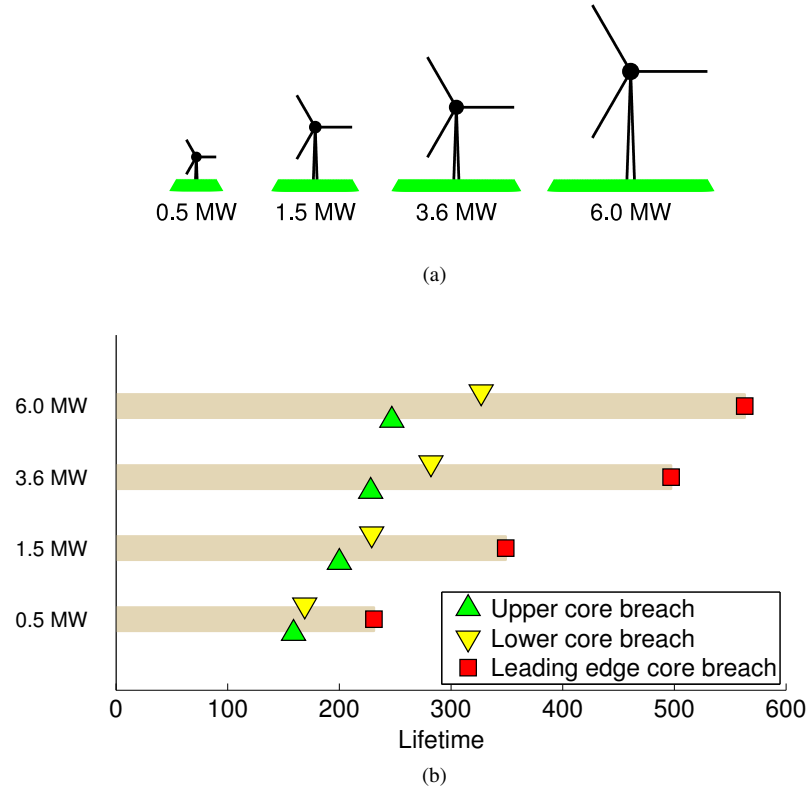


**Figure 12. Turbine size parametric study: (a) comparison of wind turbines and (b) blade section lifetime versus turbine size.**

sand erosion is depicted in Fig. 12(b) on the  $x$ -axis, and the turbine rated power is on the  $y$ -axis. The bars represent the lifespan of the blade and the intermediate markers represent the relevant milestones through it (Phase 1, 2, and 3). A dramatic increase in turbine lifetime is observed when increasing the wind turbine rated power. In particular, a 0.5 MW HAWT has about one third the lifespan of a modern 6.0 MW HAWT. Such results can be explained by considering the effect of hub height with respect to sand erosion, as explained in Sec. V C. However, the biggest contribution to an increase in lifetime is due to the large chord lengths typical of large wind turbines. In fact, when a particle approaches a large-chord airfoil, it will be exposed to the perturbed flowfield sooner and will therefore have more time to stay aligned with the streamlines thereby resulting in less erosion. Small wind turbines do not favor such effects and therefore are subject to a more intense erosion, thus reducing their lifespan. The present result is a novelty in the wind turbine field, and may be thought as another important reason to favor large wind turbines.

### E. Effect of Airfoil Geometry on Blade Lifetime

Ultimately, the erosion on a wind turbine depends on the airfoil geometry.<sup>41</sup> In particular, the role of the suction peak on the upper side, along with the leading edge curvature are important factors that drive the maximum erosion rate and the location of  $E_{max}$ . In the current Section, multiple airfoils are tested to investigate the effects of various geometric features on the lifetime of the blade. Since the DU airfoil family was designed with a consistent underlying

philosophy, the pool of airfoils was expanded by including the NREL S airfoil family,<sup>66</sup> in order to have a more comprehensive parametric airfoil study.

Along with the DU 96-W-180, the selected airfoils were the NREL S804, S810, S813, S817, S820, S821, S828, and S832. These airfoils were specifically designed for wind turbine applications in the 90's, and they all have similar  $t/c$  ( $\approx 18\%$ ). They were however not designed for a common blade span location.<sup>66</sup> The focus of the current analysis is to highlight the geometric features that favor blade lifespan, therefore such airfoils were evaluated nevertheless. Figure 13(a) shows an overall comparison of the airfoils, and Fig. 13(b) shows the variety in leading edge geometry within the pool of airfoils.

All simulations were performed at a constant  $C_l = 1.0$  while the considered blade section was located at  $r/R = 0.95$ . Figure 14 shows the lifetime of the various airfoils, and the adopted graphic layout is the same as in Sec. V D. It can be readily noticed that there exists a similar lifetime before the upper core breach among all airfoils. However, the only airfoil to have a significantly delayed upper core breach is the NREL S804. It is worth noticing from Fig. 13(b) that such an airfoil shows the most bulbous leading edge among the tested geometries. Thus, because the suction peak is significantly reduced and moved downstream for this geometry, the upper core breach occurs the latest. Interestingly, NREL S804 also shows the longest lifetime before the leading edge core breach. This can be explained by the forward part of the airfoil offering large impact angles to the incoming particles, thus reducing the erosion rate.

The analysis of the bar chart in Fig. 14 allows for another important observation. In a theoretical rank of the airfoils based on their lifetime before leading edge core breach, the NREL S804 airfoil would come first, followed by the NREL S813, and by the DU 96-W-180. However, the reason behind such positive performance of the NREL S813 airfoil is not strictly related to the geometry of the leading edge. In fact, by inspecting Fig. 13(b), the geometry of the leading edge does not appear particularly bulbous, and yet the airfoil ranks second in the chart. The reason behind this result has to be found in the aft camber of the airfoil, as shown in Fig. 13(a). Given a prescribed  $C_l$ , the airfoil camber can be increased to reduce the angle of attack to achieve the target lift coefficient. When camber is localized in the aft portion of the airfoil it allows for a reduction of the suction peak on the upper side of the leading edge, thus favoring the blade section lifespan.

The present Section highlights the role of airfoil geometry with respect to blade lifespan. In general, the leading edge curvature combined with the airfoil camber represent two geometric drivers of the blade lifespan. Such a result is novel and may serve as a technical insight for airfoil designers who are interested in extending the blade lifespan and mitigating the erosive effects of sand. Note that similar recommendations for airfoil design were also outlined in Ref. 41.

## F. Erosive Patterns

The lessons learned by implementing and using the time-stepping code can translate into practical directions for wind turbine blade maintenance. In fact, it can be assumed that by regularly inspecting the surface of a real blade affected by heavy sand grain erosion, the following phases would be observed:

1. At the earliest stage, thin orderly scratches on the blade would be observed in the regions predicted by the inviscid computations, where the surface displacement  $\delta$  is maximum. The highest density and depth of such scratches would appear on the blade upper surface, in close proximity of the leading edge. Scratches would also appear shortly after on the blade lower side.
2. As the damage progresses, a reduced coating thickness would be observed where the predicted  $\delta$  is maximum. At the same time, an increased roughness would be observed close to the blade leading edge; whereas, a smaller increment of scratches would be seen downstream. It can be postulated that the increase in surface roughness due to sand erosion may promote transition to turbulent flow, thus increasing the chances for the lightweight particles to be transported away from the surface by means of funnel structures and turbulent flow motion.<sup>40,67-69</sup> This effect would help the erosive damage not to progress further downstream on the surface.
3. The progressive transition of the boundary layer would be completed at this phase. Because the blade coating is completely removed at the locations of maximum  $\delta$ , it can be assumed that the flow is practically turbulent starting at such locations. At this stage, little variations in the observed damage downstream of those locations would be observed. Conversely, the damage on the very leading edge would increase, and potentially be worsened by long-term coating fatigue mechanisms and impact with heavy particles such as hailstones, rain drops, or insects.

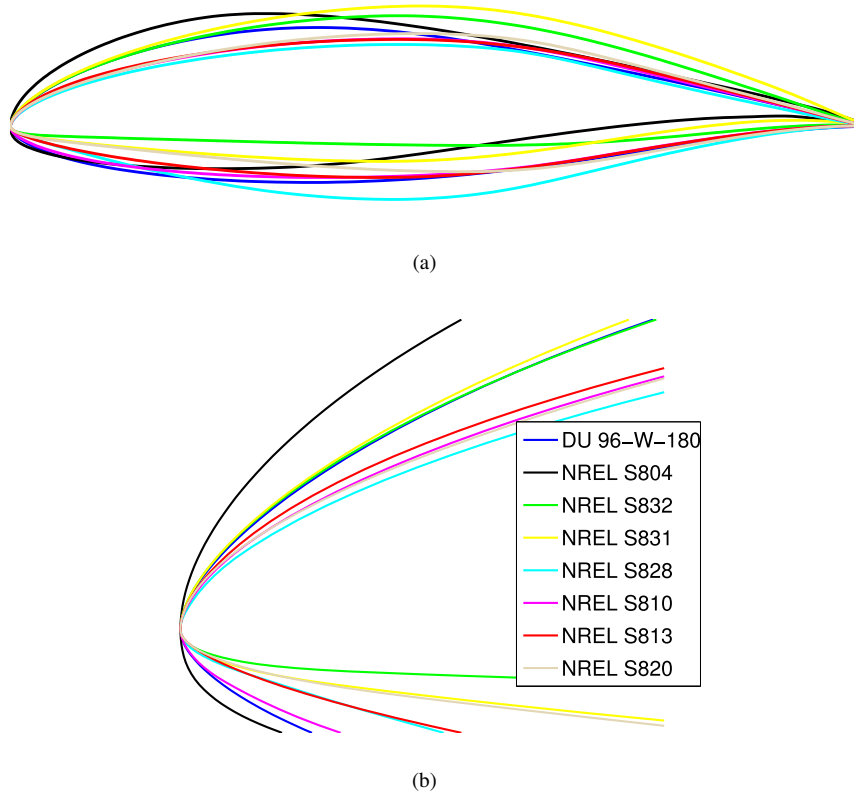


Figure 13. Selected pool of airfoils: (a) overall comparison, and (b) zoom-in on the leading edge region.

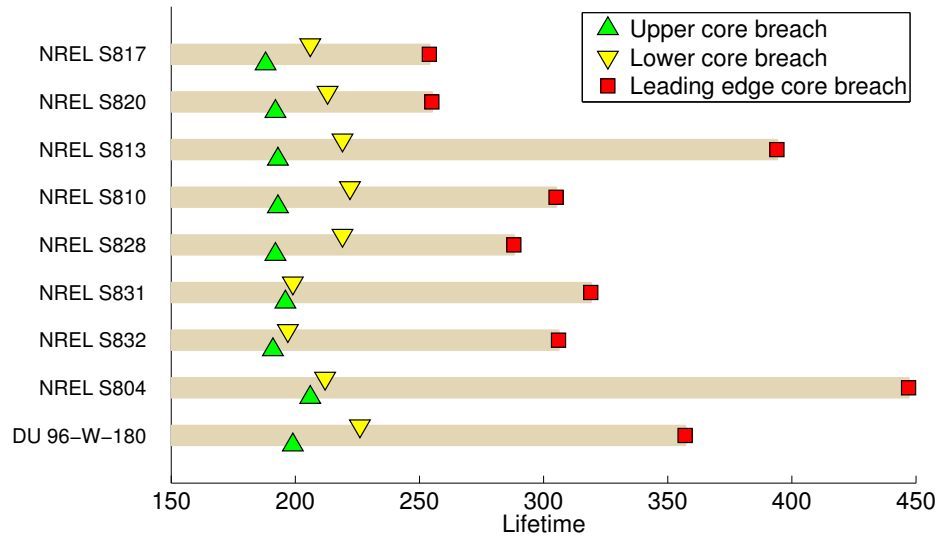


Figure 14. Blade section lifetime with respect to airfoil geometry

4. The damage patterns would unlikely enlarge their boundaries downstream of the transition locations; whereas, an in-depth damage pattern may occur in the surroundings of the uncoated blade leading edge. At that location, the surface may be subject to a more intense deterioration due to the less erosion-resilient core materials of the blade.

## VI. Conclusions

The present paper describes the implementation of a time-stepping algorithm to predict the final shape of wind turbine blade sections subject to sand erosion. Even if great uncertainties exist as far as sand grain size and distribution through the earth atmosphere, realistic eroded geometries were produced and compared reasonably with photographic evidence. Three main phases were identified through the blade lifespan: an upper core breach, a lower core breach, and a leading edge core breach. An extensive parametric study allowed to determine the most relevant drivers of the blade lifespan. In particular, the sand grain diameter was found to be the most significant driver, and the lifespan of the blade decreases parabolically as the grain diameter increases. Moreover, both the lift coefficient and the turbine hub height showed a direct relationship with blade lifespan. Large lift coefficients and large turbine hub heights are beneficial toward blade lifespan. It was also found that modern, large wind turbines are affected consistently less by sand erosion than small wind turbines. Such an effect is due to the increased influence of the blade flowfield toward a deviation of the incoming particles when large blade chord lengths are involved, but also to the reduced sand grain diameter at high elevations off the ground. Finally, a survey of various airfoil geometries allowed to identify the shape of the leading edge along with the airfoil aft camber as the primary drivers of blade section lifespan. Bulbous and round leading edges, coupled with moderately aft-cambered airfoils allowed for the longest blade lifespans observed as they reduce the blade upper suction peak and offer steeper impact angles to the particles.

## VII. Acknowledgments

The author would like to thank Chandan Vempati, Nicholas Fulton, and Yu Cai for their interest and help during the development of the time marching code.

## References

- <sup>1</sup>Dalili, N., Edrisy, A., and Carriveau, R., "A Review of Surface Engineering Issues Critical to Wind Turbine Performance," *Renewable and Sustainable Energy Reviews*, Vol. 13, 2007, pp. 428–438.
- <sup>2</sup>Sagol, E., Reggio, M., and Ilinca, A., "Issues Concerning Roughness on Wind Turbine Blades," *Renewable and Sustainable Energy Reviews*, Vol. 23, 2013, pp. 514–525.
- <sup>3</sup>Ahmed, M. R., "Blade Sections for Wind Turbine and Tidal Current Turbine Applications – Current Status and Future Challenges," *International Journal of Energy Research*, Vol. 36, 2012, pp. 829–844.
- <sup>4</sup>Hayman, B., Wedel-Heinen, J., and Brondsted, P., "Materials Challenges in Present and Future Wind Energy," *MRS Bulletin*, Vol. 33, April 2008, pp. 343–353.
- <sup>5</sup>Singh, S., Bhatti, T. S., and Kothari, D. P., "A Review of Wind-Resource-Assessment Technology," Centre for Energy Studies, Indian Institute of Technology, Hauz Khas, New Delhi 110016, 2012.
- <sup>6</sup>Ciang, C. C., Lee, J. R., and Bang, H. J., "Structural Health Monitoring for a Wind Turbine System: a Review of Damage Detection Methods," *Measurement Science and Technology*, Vol. 19, No. 12, Oct. 2008, pp. 122001–122021.
- <sup>7</sup>Huang, C. W., Yang, K., Liu, Q., Zhang, L., Bai, J. Y., and Xu, J. Z., "A Study on Performance Influences of Airfoil Aerodynamic Parameters and Evaluation Indicators for the Roughness Sensitivity on Wind Turbine Blade," *Science China - Technological Sciences*, Vol. 54, No. 11, 2011, pp. 2993–2998.
- <sup>8</sup>Mayor, G. S., Moreira, A. B. B., and Munoz, H. C., "Influence of Roughness in Protective Strips of Leading Edge for Generating Wind Profiles," *22nd International Congress of Mechanical Engineering, COBEM 2013*, 2013.
- <sup>9</sup>Soltani, M. R., Birjandi, A. H., and Seddighi-Moorani, M., "Effect of Surface Contamination on the Performance of a Section of a Wind Turbine Blade," *Scientia Iranica B*, Vol. 18, No. 3, 2011, pp. 349–357.
- <sup>10</sup>Ren, N. and Ou, J., "Dust Effect on the Performance of Wind Turbine Airfoils," *Journal of Electromagnetic Analysis and Applications*, Vol. 1, No. 2, 2009, pp. 102–107.
- <sup>11</sup>Sareen, A., Sapre, C. A., and Selig, M. S., "Effects of Leading-Edge Protection Tape on Wind Turbine Blade Performance," *Wind Engineering*, Vol. 36, No. 5, 2012, pp. 525–534.
- <sup>12</sup>van Rooij, R. P. J. O. M. and W.A.Timmer, "Roughness Sensitivity Considerations for Thick Rotor Blade Airfoils," *Proceedings of the 41st Aerospace Sciences Meeting and Exhibit*, AIAA Paper 2003-350, 2003.
- <sup>13</sup>Arrighetti, C., Pratti, G. D., and Ruscitti, R., "Performance Decay Analysis of New Rotor Blade Profiles for Wind Turbines Operating in Offshore Environments," *Wind Engineering*, Vol. 27, No. 5, 2003, pp. 371–380.

- <sup>14</sup>Ragheb, A. and Selig, M. S., "Multi-Element Airfoil Configurations for Wind Turbines," *Proceedings of the 29th AIAA Conference*, AIAA Paper 2011-3971, 2011.
- <sup>15</sup>Schneiderhan, T., Schulz-Stellenfleth, J., Lehner, S., and Hortsman, J., "Sar Wind Fields for Offshore Wind Farming," DLR, Oberpfaffenhofen, 82230 Wessling, Germany, 2002.
- <sup>16</sup>DNV, "Design and Manufacture of Wind Turbine Blades, Offshore and Onshore Wind Turbines - October 2010," Standard DNV-DS-J102, Det Norske Veritas, Oct 2010.
- <sup>17</sup>Khakpour, Y., Bardakji, S., and Nair, S., "Aerodynamic Performance of Wind Turbine Blades in Dusty Environments," *International Mechanical Engineering Congress and Exposition, Seattle, Washington*, IMECE2007-43291, 2007.
- <sup>18</sup>Tilly, G., "Erosion Caused by Airborne Particles," *Wear*, Vol. 14, No. 1, 1969, pp. 63–79.
- <sup>19</sup>Davis, J. R., editor, *Surface Engineering for Corrosion and Wear Resistance*, chap. 3, ASM International - The Materials Information Society, 10M Communications, Materials Park, OH 44073-0002, 2001, pp. 43–86.
- <sup>20</sup>Wood, R. J. K., "The Sand Erosion Performance of Coatings," *Materials and Design*, Vol. 20, No. 4, 1999, pp. 179–191.
- <sup>21</sup>Tabakoff, W. and Balan, C., "A Study of the Surface Deterioration due to Erosion," *Presented at the 28th ASME International Gas Turbine Conference and Exhibit*, Vol. 105, 1983, pp. 834–838.
- <sup>22</sup>Fiore, G. and Selig, M. S., "A Simulation of Operational Damage for Wind Turbines," *Proceedings of the 32nd AIAA Applied Aerodynamics Conference*, AIAA Paper 2014–2848, Atlanta, GA, 2014.
- <sup>23</sup>Fiore, G., Fujiwara, G. E. C., and Selig, M. S., "A Damage Assessment for Wind Turbine Blades from Heavy Atmospheric Particles," *Proceedings of the AIAA Conference*, AIAA Paper 2015–1495, Kissimmee, FL, 2015.
- <sup>24</sup>Keegan, M. H., Nash, D. H., and Stack, M. M., "On Erosion Issues Associated with the Leading Edge of Wind Turbine Blades," *Journal of Physics D: Applied Physics*, Vol. 46, 2013, pp. 1–20.
- <sup>25</sup>Keegan, K. H., Nash, D. H., and Stack, M. M., "Modelling Rain Drop Impact of Offshore Wind Turbine Blades," *Proceedings of the TURBO EXPO*, 2012.
- <sup>26</sup>Keegan, K. H., Nash, D., and Stack, M., "Numerical Modelling of Hailstone Impact on the Leading Edge of a Wind Turbine Blade," Workshop paper, University of Strathclyde, Department of Mechanical and Aerospace Engineering, 2013.
- <sup>27</sup>Edwards, R. and Hodanish, S. J., "Photographic Documentation and Environmental Analysis of an Intense, Anticyclonic Supercell on the Colorado Plains," *Monthly Weather Review - Picture of the Month*, Vol. 135, 2006, pp. 3753–3763.
- <sup>28</sup>Changnon, S. A., "Data and Approaches for Determining Hail Risk in the Contiguous United States," *Journal of Applied Meteorology*, Vol. 38, 1999, pp. 1730–1739.
- <sup>29</sup>Macdonald, H., Infield, D., Nash, D. H., and Stack, M. M., "Mapping Hail Meteorological Observations for Prediction of Erosion in Wind Turbines," *Wind Energy*, 2015, pp. 1–8.
- <sup>30</sup>Bak, C., Madsen, H. A., Fuglsang, P., and Rasmussen, F., "Observations and Hypothesis of Double Stall," *Wind Energy*, Vol. 2, 1999, pp. 195–210.
- <sup>31</sup>Corten, G. and Veldkamp, H., "Insects Can Cause Double Stall," Technical Report, Energy Centre of the Netherlands ECN, Westerduinweg 3, NL 1755 ZG Petten, 2001.
- <sup>32</sup>Bragg, M. B., "Rime Ice Accretion and Its Effect on Airfoil Performance," NASA CR-165599, Mar 1982.
- <sup>33</sup>Khalfallah, M. G. and Koliub, A. M., "Effect of Dust on the Performance of Wind Turbines," *Desalination*, Vol. 209, 2007, pp. 209–220.
- <sup>34</sup>Yang, X. H., Xu, X. L., He, Q., Mamtimin, A., Yu, B., and Tang, S. H., "Sand Flux Estimation During a Sand-Dust Storm at Tazhong Area of Taklimakan Desert, China," *Journal of Arid Land*, Vol. 3, No. 3, 2011, pp. 199–205.
- <sup>35</sup>Li, Z. S., Feng, D. J., Wu, S. L., Borthwick, A. G. L., and Ni, J. R., "Grain Size and Transport Characteristics of Non-Uniform Sand in Aeolian Saltation," *Geomorphology*, Vol. 100, 2008, pp. 484–493.
- <sup>36</sup>Ahmed, A. S., Ali, A. A., and Alhaider, M. A., "Measurement of Atmospheric Particle Size Distribution During Sand/Duststorm in Riyadh, Saudi Arabia," *Atmospheric Environment*, Vol. 21, 1987, pp. 2723–2725.
- <sup>37</sup>Gu, Y., Rose, W. I., and Bluth, G. J. S., "Retrieval of Mass and Sizes of Particles in Sandstorms Using Two MODIS IR Bands: A Case Study of April 7, 2001 Sandstorm in China," *Geophysical Research Letters*, Vol. 30, No. 15, 2003, pp. 1–4.
- <sup>38</sup>Wood, K., "Blade Repair: Closing the Maintenance Gap," *Composites World*, Apr 2011, <http://www.compositesworld.com>.
- <sup>39</sup>Challener, C., "Coatings Critical for Wind Energy Efficiency," *JCT CoatingsTech*, Jan 2010.
- <sup>40</sup>Kerho, M. F. and Bragg, M. B., "Airfoil Boundary-Layer Development and Transition with Large Leading-Edge Roughness," *AIAA*, Vol. 35, No. 1, 1997, pp. 75–84.
- <sup>41</sup>Fiore, G. and Selig, M. S., "Optimization of Wind Turbine Airfoils Subject to Particle Erosion," *Proceedings of the 33rd AIAA Applied Aerodynamics Conference*, AIAA Paper 2015–3393, Dallas, TX, 2015.
- <sup>42</sup>Sareen, A., Sapre, C. A., and Selig, M. S., "Effects of Leading Edge Erosion on Wind Turbine Blade Performance," *Wind Energy*, Vol. 17, 2014, pp. 1531–1542.
- <sup>43</sup>Bragg, M. B. and Maresh, J. L., "A Numerical Method To Predict The Effect of Insect Contamination on Airfoil Drag," Aeronautical and Astronautical Engineering Report AARL 86-01, The Ohio State University Research Foundation, Columbus, OH 43212, Mar 1986.
- <sup>44</sup>Drela, M., "XFoil: An Analysis and Design System for Low Reynolds Number Airfoils," *Low Reynolds Number Aerodynamics*, edited by T. J. Mueller, Vol. 54 of *Lecture Notes in Engineering*, Springer-Verlag, New York, June 1989, pp. 1–12.
- <sup>45</sup>Roskam, J., *Airplane Flight Dynamics and Automatic Flight Controls*, DARcorp, Lawrence, KS 66044, 1995.
- <sup>46</sup>Langmuir, I. and Blodgett, K., "Mathematical Investigation of Water Droplet Trajectories," Tech. Rept. 5418, U.S. Army Air Force, 1946.
- <sup>47</sup>Hamed, A. A., Tabakoff, W., Rivir, R. B., Das, K., and Arora, P., "Turbine Blade Surface Deterioration by Erosion," *Journal of Turbomachinery*, Vol. 127, No. 3, 2005, pp. 445–452.
- <sup>48</sup>Haider, A. and Levenspiel, O., "Drag Coefficient and Terminal Velocity of Spherical and Nonspherical Particles," *Powder Technology*, Vol. 58, No. 1, 1989, pp. 63–70.
- <sup>49</sup>Feuerstein, A. and Kleymann, A., "Ti-N Multilayer Systems for Compressor Airfoil Sand Erosion Protection," *Surface and Coatings Technology*, Vol. 204, No. 6–7, 2009, pp. 1092–1096.

- <sup>50</sup>Maozhong, Y., Baiyun, H., and Jiawen, H., "Erosion Wear Behaviour and Model of Abradable Seal Coating," *Wear*, Vol. 252, No. 1–2, 2002, pp. 9–15.
- <sup>51</sup>J. Zahavi and G. F. Schmitt Jr., "Solid Particle Erosion of Polymeric Coatings," *Wear*, Vol. 71, No. 2, 1981, pp. 191–210.
- <sup>52</sup>Arjula, S., Harsha, A. P., and Ghosh, M. K., "Solid-particle Erosion Behavior of High-Performance Thermoplastic Polymers," *Journal of Material Science*, Vol. 43, No. 6, 2008, pp. 1757–1768.
- <sup>53</sup>Harsha, A. P. and Thakre, A. A., "Investigation on Solid Particle Erosion Behaviour of Polyetherimide and its Composites," *Wear*, Vol. 262, No. 7–8, 2007, pp. 807–818.
- <sup>54</sup>Barkoula, N.-M. and Karger-Kocsis, J., "Review – Processes and Influencing Parameters of the Solid Particle Erosion of Polymers and Their Composites," *Journal of Materials Science*, Vol. 37, 2002, pp. 3807–3820.
- <sup>55</sup>Arjula, S. and Harsha, A. P., "Study of Erosion Efficiency of Polymers and Polymer Composites," *Polymer Testing*, Vol. 25, No. 2, 2006, pp. 188–196.
- <sup>56</sup>Patnaik, A., Satapathy, A., and Mahapatra, S. S., "A Modeling Approach for Prediction of Erosion Behavior of Glass Fiber-Polyester Composites," *Journal of Polymer Research*, Vol. 15, No. 2, 2008, pp. 147–160.
- <sup>57</sup>Frost, W. and Aspliden, C., "Characteristics of The Wind," *Wind Turbine Technology, Fundamental Concepts of Wind Turbine Engineering, Second Edition*, edited by D. A. Spera, ASME Press, Three Park Avenue, New York City, NY 10016, 2009, pp. 467–541.
- <sup>58</sup>ISL, "Blade Repair," ISL Wind, Nov 2014, <http://www.islwind.com/Blade-Repair.html>.
- <sup>59</sup>Leaverton, G. and Parle, J., "AAIR Team – Wind Energy Presentation," New Ideas for Trimming O&M Costs, Windpower Engineering and Development – Webinar Series, Jan 2015, <http://www.windpowerengineering.com>.
- <sup>60</sup>Hogre Hojder AB, "Wind turbine rotor blade: Inspection and repair," Hogre Hojder AB, Mar 2015, <http://www.hogrehojder.se/windturbineEN.html>.
- <sup>61</sup>Rempel, L., "Rotor Blade Leading Edge Erosion - Real Life Experiences", Oct 2012, <http://www.windsystemsmag.com>.
- <sup>62</sup>Corsini, A., Marchegiani, A., Rispoli, F., Venturini, P., and Sheard, A. G., "Predicting Blade Leading Edge Erosion in an Axial Induced Draft Fan," *Journal of Engineering for Gas Turbines and Power*, Vol. 134, 2012, pp. 1–9.
- <sup>63</sup>Wilson, R. E., "Wind Turbine Aerodynamics Part A: Basic Principles," *Wind Turbine Technology, Fundamental Concepts of Wind Turbine Engineering, Second Edition*, edited by D. A. Spera, ASME Press, Three Park Avenue, New York City, NY 10016, 2009, pp. 281–350.
- <sup>64</sup>Hatch, G., "Why Are Wind Turbines Getting Bigger?," Aug 2009, <http://www.terramagnetica.com>.
- <sup>65</sup>Vella, H., "In Pictures - The World's Longest Wind Turbine Rotor Blades", Jun 2013, <http://www.power-technology.com>.
- <sup>66</sup>Tangler, J. L., "The Evolution of Rotor and Blade Design," *Presented at the American Wind Energy Association, Wind Power 2000*, NREL CP-500-28410, 2000.
- <sup>67</sup>Kaftori, D., Hetsroni, G., and Banerjee, S., "Particle Behavior in the Turbulent Boundary Layer. I. Motion, Deposition and Entrainment," *American Institute of Physics*, Vol. 7, No. 5, 1995, pp. 1095–1106.
- <sup>68</sup>Kaftori, D. and Banerjee, S., "Particle Behavior in the Turbulent Boundary Layer. II. Velocity and Distribution Profiles," *American Institute of Physics*, Vol. 7, No. 5, 1995, pp. 1107–1121.
- <sup>69</sup>Sardina, G., Brandt, L., Schlatter, P., Casciola, C. M., and Henningson, D., "Transport of Inertial Particles in Turbulent Boundary Layers," *13th European Turbulence Conference*, No. 318, Journal of Physics: Conference Series, 2013.